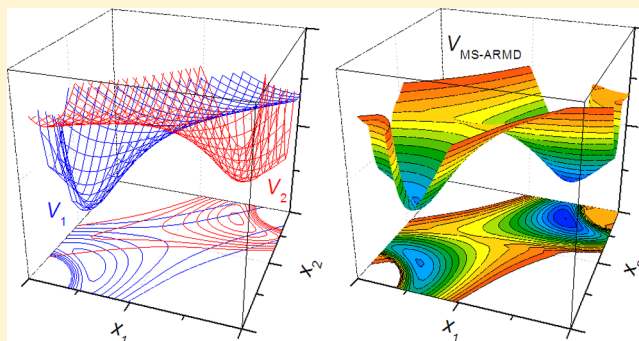


Multisurface Adiabatic Reactive Molecular Dynamics

Tibor Nagy,* Juvenal Yosa Reyes, and Markus Meuwly*

Department of Chemistry, University of Basel, 4056 Basel, Switzerland

ABSTRACT: Adiabatic reactive molecular dynamics (ARMD) simulation method is a surface-crossing algorithm for modeling chemical reactions in classical molecular dynamics simulations using empirical force fields. As the ARMD Hamiltonian is time dependent during crossing, it allows only approximate energy conservation. In the current work, the range of applicability of conventional ARMD is explored, and a new multisurface ARMD (MS-ARMD) method is presented, implemented in CHARMM and applied to the vibrationally induced photodissociation of sulfuric acid (H_2SO_4) in the gas phase. For this, an accurate global potential energy surface (PES) involving 12 H_2SO_4 and 4 $\text{H}_2\text{O} + \text{SO}_3$ force fields fitted to MP2/6-311G++(2d,2p) reference energies is employed. The MS-ARMD simulations conserve total energy and feature both intramolecular H-transfer reactions and water elimination. An analytical treatment of the dynamics in the crossing region finds that conventional ARMD can approximately conserve total energy for limiting cases. In one of them, the reduced mass of the system is large, which often occurs for simulations of solvated biomolecular systems. On the other hand, MS-ARMD is a general approach for modeling chemical reactions including gas-phase, homogeneous, heterogeneous, and enzymatic catalytic reactions while conserving total energy in atomistic simulations.



1. INTRODUCTION

Following the dynamics and energetics of chemical reactions is of fundamental importance in all branches of chemistry and biology. Experimentally, reaction mechanisms often need to be inferred from phenomenological kinetic models because simultaneous determination of the physical trajectories of the participating particles and their energetics is typically not possible. Hence, computational methods play an essential role in elucidating, at atomic resolution, the possible reaction pathways followed for a particular chemical reaction. Analysis of the atoms' trajectories ultimately provides deeper insight about the sequence of events that connect reactants (educts) and products and are therefore the most elementary level at which reaction mechanisms can be analyzed and understood.

The most rigorous computational treatment of such processes uses quantum methods for the electronic structure and nuclear dynamics. However, this is usually impractical due to the computational requirements. Alternatively, the nuclear motion can be treated quantum mechanically while using a parametrized potential energy surface (PES). This has been successfully done for a number of topical systems.^{1–6} As a thermal rate constant is an ensemble average over a large number of initial conditions, a statistically significant number of trajectories needs to be run and analyzed. Therefore, approaches that treat the nuclear dynamics at the classical level have become an attractive and often meaningful alternative. Such simulations can, under favorable circumstances, be run by resorting to quantum mechanical (QM)^{7–9} or mixed quantum/molecular mechanics (QM/MM) treat-

ments.^{10–12} Alternatively, if empirical and fully dimensional force fields of sufficient accuracy can be parametrized, they offer a viable means to exhaustively sample phase space from which meaningful rate parameters can be determined.^{13–18}

Over the past few years, a number of approaches have been developed that use empirical force fields for following chemical reactions in the gas phase and in solution. One of them is the empirical valence bond (EVB) technique that was particularly relevant to (proton transfer) reactions in solution.¹³ The generalization of EVB to multistate EVB has played an important role for investigating proton transfer in solution.¹⁹ The EVB Hamiltonian usually consists of two or more diagonal terms that are force field expressions for all states of interest. The off-diagonal terms are coupling matrix elements that depend parametrically on one (or several) internal coordinates of the system.²⁰ This introduces a dependence on the choice of the coordinates that is not always desirable, e.g., if multiple bond rearrangements can occur. Alternatively, a chemical reaction can be followed along time as the progression coordinate, which is the situation encountered in experiments.^{21,22} This is the purpose of adiabatic reactive molecular dynamics (ARMD) that was originally developed for reactions in the condensed phase.^{14,15,21,23} More recently, ARMD has also been applied to gas-phase systems such as the vibrationally induced photodissociation of sulfuric acid (H_2SO_4). Here, the excitation of a higher overtone ($\nu_9 \geq 4$) of a local OH-

Received: October 31, 2013

Published: March 10, 2014

stretching vibration can lead to photodissociation into water and sulfur-trioxide ($\text{H}_2\text{O} + \text{SO}_3$) on the picosecond to nanosecond time scale.^{17,24} However, the ARMD trajectories were not suitable for final state analysis of the reaction products because they were based on an explicitly time-dependent Hamiltonian that does not conserve total energy during crossing.

Because significant energy conservation violation was observed during crossing in gas-phase reactions, ARMD was modified to multisurface ARMD (MS-ARMD) that allows reactive molecular dynamics simulations that conserve total energy.²⁵ It has already been successfully applied to the charge transfer reaction $\text{N}_2^+ + \text{N}_2 \rightarrow \text{N}_2 + \text{N}_2^+$ and explain recent experimental findings based on an accurate global adiabatic potential energy surface (PES).²⁵ The reaction at the investigated conditions involves the formation of a vibrationally highly excited $[\text{N}-\text{N}\cdots\text{N}-\text{N}]^+$ complex with lifetimes on the 1 to 100 ps time scale during which several bond rearrangements take place. The study required 24 force fields (FFs) to construct a permutationally invariant global PES capable of describing all atom arrangements within the complex that can evolve into the various final states.²⁵ That work served as a validation study, and the general underlying concepts are discussed in the present work together with an application to the decomposition reaction of H_2SO_4 involving competing pathways.

This work is structured as follows. In Section 2, the original ARMD implementation is explored for its applicability and generalized to multisurface ARMD (MS-ARMD) in section 3. Finally, the methodology is applied to the vibrationally induced photodissociation of H_2SO_4 , which is a suitable test system for several reasons. First, it offers the possibility of investigating competing pathways, including intramolecular H-transfer and water elimination. Both processes have been found in earlier MD simulations at the semi-empirical level.²⁴ Second, the process is expected to occur on the picosecond to nanosecond time scale that allows us to exhaustively sample phase space prior to excitation and to follow the subsequent dissociation dynamics. Furthermore, the lack of an observable dissociative electronic state of H_2SO_4 has ruled out UV photochemistry as the explanation for the springtime polar stratospheric sulfate layer, which requires production of SO_2 from H_2SO_4 .^{26–29} For this, a mechanism based on vibrationally induced photodissociation of $\text{H}_2\text{SO}_4 \rightarrow \text{SO}_3 + \text{H}_2\text{O}$ has been proposed.²⁹ Hence, the system considered here provides the necessary balance of complexity and tractability required for a rigorous validation of MS-ARMD. Finally, comparisons with other existing methods are made and conclusions are drawn.

2. ADIABATIC REACTIVE MOLECULAR DYNAMICS AND ITS APPLICABILITY

2.1. ARMD Procedure. Adiabatic reactive molecular dynamics (ARMD) is a surface-crossing method to follow bond-breaking and forming processes using empirical force fields.^{14,21} In ARMD, at least two parametrized potential energy surfaces (PESs), V_1 for the educt and V_2 for the product states, are considered. The adiabatic dynamics of the nuclei takes place on the lowest PES while the energy of the higher state(s) is also determined. Whenever the energy of the current state (which is V_1 in Figure 1) equals that of a higher PES, the simulation is restarted a few time steps prior to the detected crossing. Following this, the method interpolates on-the-fly between the two PESs.^{14,21} During a finite time interval t_s , called switching

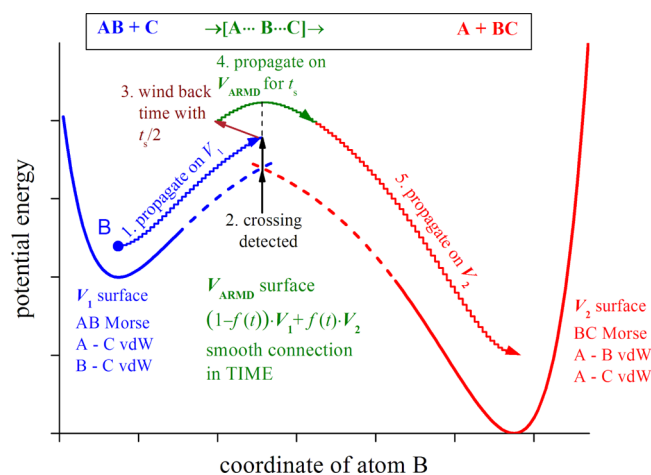


Figure 1. Algorithm of Adiabatic Reactive Molecular Dynamics (ARMD) simulation method is schematically shown in five steps for collinear atom transfer reaction (atom B is transferred) where the coordinates of donor (A) and acceptor (C) atoms are fixed. During the crossing, the surfaces are switched in time, and the Morse bond is replaced by van der Waals (vdW) interactions and vice versa.

time (typically a few fs), which is largely determined by the process in question, the PESs are mixed in different proportions by multiplying them with a suitable time-dependent switching function $f(t)$ (e.g., a tanh function). With reference to Figure 1, at the beginning of the mixing, the system is fully described by V_1 ($f(t) = 0$), while at the end it evolves to V_2 ($f(t) = 1$). One of the particular advantages of ARMD is that the reaction develops with time as the progression coordinate, which is a “natural” choice. Thus, no definition of a necessarily approximate reaction coordinate, which even might change as the reaction progresses, is required. The algorithm of ARMD is schematically shown for a collinear atom transfer reaction in Figure 1.

As during surface crossing, the ARMD potential energy is explicitly time dependent, the total energy of the system cannot be conserved in a strict sense (see below). For large systems (e.g., proteins in solution), total energy was found to be conserved to within ≈ 1 kcal/mol, which is sufficient for most applications.^{14,21} However, for small systems in the gas phase, this is not necessarily true. In cases where only the reaction time is of interest (i.e., the time to reach the transition state), exact energy conservation is not necessarily required. This was the case for vibrationally induced photodissociation of H_2SO_4 .¹⁷ If, however, several crossings between the states involved can take place or the course of the dynamics after the reaction is of interest, e.g., for a final state analysis, energy conservation becomes crucial.

2.2. Applicability of ARMD. To explore the range of applicability of the ARMD method, an approximate expression for the amount of energy violation is derived and analyzed in the following. For this, we consider a curve crossing between two one-dimensional PESs $V_1(x)$ and $V_2(x)$. In ARMD, the dynamics in the crossing region evolves on a mixed, explicitly time-dependent PES on the interval $(0, t_s)$

$$V_{\text{ARMD}}(x, t) = (1 - f(t))V_1(x) + f(t)V_2(x) \quad (1)$$

For the situation in Figure 2, the two 1D PESs cross at $x = 0$. The following analysis starts from a linear approximation of the PESs that is valid sufficiently close to the crossing point ($V_1(x) = \alpha x$ and $V_2(x) = \beta x$, where $\alpha > 0$ and $\beta < 0$). For the switching

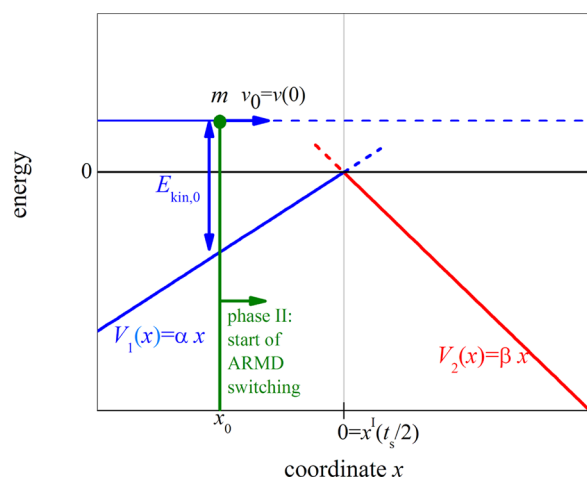


Figure 2. Simple model for estimating energy violation in ARMD simulations. The system (effective mass m) is approaching from the left on PES $V_1(x)$ (phase I). At time $t = 0$ the system is at x_0 with velocity v_0 and kinetic energy $E_{\text{kin},0}$. After crossing is detected at $x = 0$, the time is rewound by $t_s/2$, and the dynamics is resimulated while $V_1(x)$ is being switched to $V_2(x)$ during t_s (phase II).

function $f(t) = t/t_s$ is used, which is defined on the interval $(0, t_s)$ and which allows analytical treatment of the problem.

For convenience, three phases are defined. During phase I, the system is completely described by V_1 , which is the case prior to crossing. Once a crossing has been detected, phase II is entered. After completing the crossing procedure, the system is fully described by V_2 , which corresponds to phase III. As the motion during phase III is regular dynamics on V_2 , it is not discussed any further. During phase I (corresponding quantities are denoted with superscript I), we consider a system with effective mass m on $V_1(x)$ (thus $F^I = -\partial_x V^I(x, t) = -\alpha$) with initial position $x_0 < 0$ and velocity $v_0 > 0$ (i.e., regular MD; Figure 2). At $t = 0$, x_0 is chosen such that the system will reach the crossing point ($x = 0$) exactly at half of the user-defined switching time ($t_s/2$).

$$\begin{aligned} x^I(t_s/2) &= 0 \\ &= x_0 + \int_0^{t_s/2} dt' \left(v_0 + \int_0^{t'} dt'' \frac{F^I}{m} \right) \\ &= x_0 + \frac{v_0}{2} t_s - \frac{\alpha}{8m} t_s^2 \end{aligned} \quad (2)$$

According to ARMD, when crossing is detected, the time is rewound by $t_s/2$, and the dynamics is restarted on the mixed PES (phase II). The ARMD potential and its partial derivatives are

$$V^{\text{II}}(x, t) = \alpha x + \frac{\beta - \alpha}{t_s} x t \quad (3)$$

$$\partial_t V^{\text{II}}(x, t) = \frac{\beta - \alpha}{t_s} x \quad (4)$$

$$F^{\text{II}}(x, t) = -\partial_x V^{\text{II}}(x, t) = -\alpha + \frac{\alpha - \beta}{t_s} t \quad (5)$$

The time evolution of the coordinates of the system during phase II follows from

$$\begin{aligned} x^{\text{II}}(t) &= x_0 + \int_0^t dt' \left(v_0 + \int_0^{t'} dt'' \frac{F^{\text{II}}(x(t''), t'')}{m} \right) \\ &= x_0 + v_0 t - \frac{\alpha}{2m} t^2 + \frac{\alpha - \beta}{6m t_s} t^3 \end{aligned} \quad (6)$$

The total energy change ΔE^{II} during the crossing period is obtained by integration of $dE^{\text{II}}/dt = \partial_t V^{\text{II}}(x, t)$, defined in eq 4, and subsequent transformation from eq 2

$$\begin{aligned} \Delta E^{\text{II}} &= \int_0^{t_s} dt \partial_t V^{\text{II}}(x(t), t) \\ &= \frac{\beta - \alpha}{t_s} \int_0^{t_s} dt x(t) \\ &= (\beta - \alpha) \left(x_0 + \frac{v_0}{2} t_s - \frac{3\alpha + \beta}{24m} t_s^2 \right) \\ &= \frac{\beta(\alpha - \beta) t_s^2}{24m} \end{aligned} \quad (7)$$

Hence, exact or nearly exact energy conservation, $\Delta E^{\text{II}} \approx 0$, can be achieved (a) if the gradients of the two PESs are the same ($\alpha \approx \beta$) or (b) if the system has a large effective mass. This is often the case in simulations of biomolecular systems, where either the moieties involved in the reaction are heavy or the reaction is coupled with rearrangement of solvation shell, which is composed of several solvent molecules, (c) for the special case where the second surface has exactly zero or a negligible slope ($\beta \approx 0$) in the crossing region, and then the positive and negative energy violations will cancel each other, (d) if the switching time goes to zero. However, for $t_s \rightarrow 0$, a smooth connection between the PESs is not possible, and numerical integrators with finite step size will cause energy violation. As the switching time is the only variable parameter during ARMD simulations, it is useful to consider a criterion for its magnitude to guarantee energy conservation. For this purpose, one may require that energy violation compared to the initial kinetic energy ($E_{\text{kin},0} = mv_0^2/2$) be small, i.e., $|\Delta E^{\text{II}}| \ll E_{\text{kin},0}$, which implies the switching time has to fulfill

$$t_s \ll (12)^{1/2} m v_0 / (|\beta(\alpha - \beta)|)^{1/2}$$

3. MULTI-SURFACE ARMD

3.1. Constructing Global PESs with MS-ARMD. If formally exact energy conservation is required, switching between the PESs should be time-independent. In the following, we present a multisurface (MS) variant of ARMD in which the weights ($w_i(\mathbf{x})$) of the PESs ($V_i(\mathbf{x})$) are also functions of all Cartesian coordinates \mathbf{x} , and thereby, the total energy can be conserved during crossing. According to MS-ARMD, the effective surface is always the lowest-energy surface ($V_{\min}(\mathbf{x}) = \min_i V_i(\mathbf{x})$), except for those geometries where other surfaces get close to it in energy (within several ΔV , see below), in which case the algorithm switches smoothly among them by changing their weights. ΔV is a user defined parameter that regulates how the weights of the PESs involved in a crossing reduce with increasing energy separation from the lowest-energy surface at a given point \mathbf{x} . It is an energy damping parameter and plays a similar role as the switching time t_s in ARMD. The optimum value of ΔV is determined during parametrization of the global PES, which is usually done by fitting it to *ab initio* data. The effective potential energy is written as a linear combination of n PESs with weights $w_i(\mathbf{x})$.

$$V_{\text{MS-ARMD}}(\mathbf{x}) = \sum_{i=1}^n w_i(\mathbf{x}) V_i(\mathbf{x})$$

$$\text{where } w_i(\mathbf{x}) = \frac{w_{i,0}(\mathbf{x})}{\sum_{j=1}^n w_{j,0}(\mathbf{x})} \quad (8)$$

The $w_i(\mathbf{x})$ are obtained by renormalizing the raw weights $w_{i,0}(\mathbf{x})$, calculated by using a simple exponential decay function of the energy difference between surface i and the minimum energy surface with a characteristic energy difference ΔV , as shown in Figure 3.

$$w_{i,0}(\mathbf{x}) = \exp\left(-\frac{V_i(\mathbf{x}) - V_{\min}(\mathbf{x})}{\Delta V}\right) \quad (9)$$

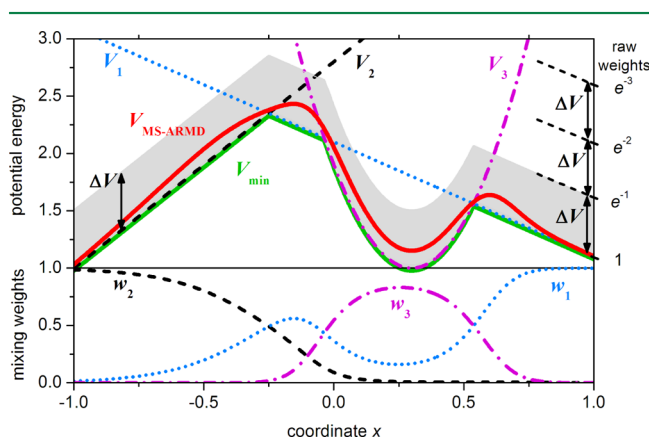


Figure 3. MS-ARMD switching method in one dimension (x) for three surfaces (V_1 , blue dotted; V_2 , black dashed; V_3 , magenta dot-dashed) defined by linear (V_1 and V_2) and quadratic (V_3) functions. The effective surface ($V_{\text{MS-ARMD}}$, red solid) always follows the lowest-energy surface (V_{\min} , green solid), except for regions where several surfaces are close in energy (within a few times $\Delta V = 0.5$). Here, the algorithm switches smoothly among them by varying their weights (w_1 , w_2 , and w_3 ; see lower panel) as a function of x . Within the grayish band above the minimum energy surface the mixing weights of surfaces drop by a factor of $e \approx 2.7$. All quantities are in arbitrary units.

Armed with the normalized weights, the global smoothed PES can be computed according to eq 8. The capabilities of MS-ARMD are illustrated for surfaces in one- and two-dimensions in Figures 3 and 4, respectively. Smooth global surfaces are obtained in all cases. The MS-ARMD surface always corresponds to the lowest PES except for regions where other surfaces are close in energy where they mix. Furthermore, the algorithm also leads to a smooth PES where more than two surfaces are close in energy, as is shown in both figures.

Equation 9 implies that for a given geometry \mathbf{x} the adiabatic PES is dominated by the contribution of the PES for which the current weight is largest (i.e., the PES with lowest energy at \mathbf{x}), whereas the contributions of all higher-lying PESs are exponentially damped. More explicitly, only those surfaces will significantly contribute to the adiabatic PES whose energies are within a few times ΔV , i.e., $V_i(\mathbf{x}) - V_{\min}(\mathbf{x}) < k\Delta V$, where k is a small integer. The term $V_{\min}(\mathbf{x})$ is necessary to avoid possible overflow and underflow in the numerical implementation of the algorithm when the raw weights of the lowest energy surfaces are calculated. This shifting term will cancel from the expressions of weights and the MS-ARMD potential energy (eq 8). Opposed to the raw weights, the final weights are analytical functions (infinitely differentiable) of the surface energies; therefore, the resulting MS-ARMD surface ($V_{\text{MS-ARMD}}(\mathbf{x})$) is a smooth function of the coordinates (\mathbf{x}).

The smooth MS-ARMD PES can be used both in Molecular Dynamics (MD) and Monte Carlo (MC) simulations. For MD simulations, the first derivative of the PES with respect to the coordinates \mathbf{x} is required and includes derivatives of the weights as well

$$\nabla V_{\text{MS-ARMD}}(\mathbf{x}) = \sum_{i=1}^n w_i(\mathbf{x}) \times \nabla V_i(\mathbf{x}) + \nabla w_i(\mathbf{x}) \times V_i(\mathbf{x}) \quad (10)$$

The new algorithm can be applied to the simultaneous switching of any number of PESs. Thus, it is possible to follow reactions that involve different pathways, such as intramolecular proton transfer and water elimination in H_2SO_4 , which is discussed below.

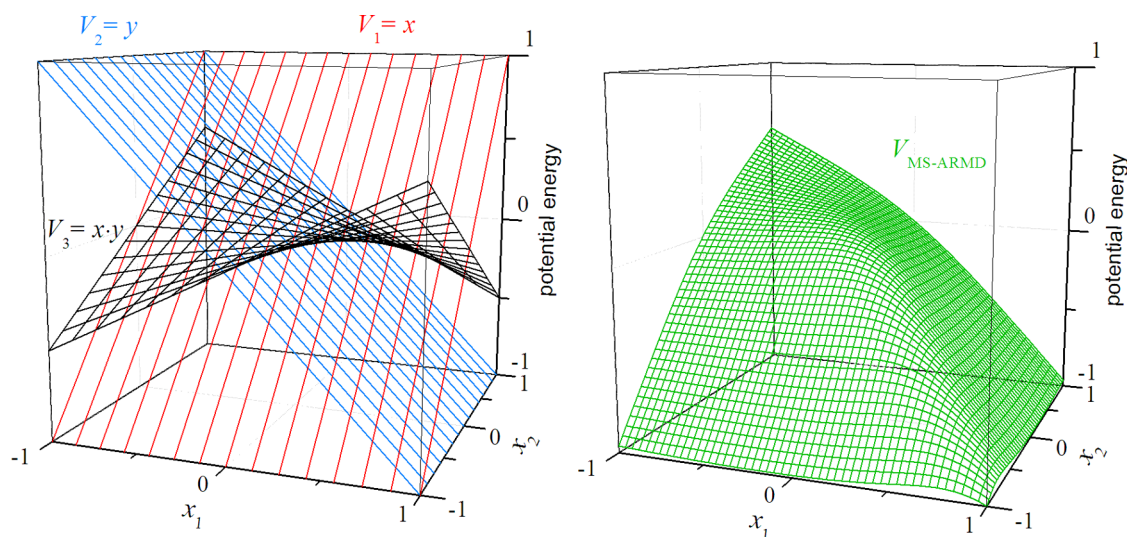


Figure 4. MS-ARMD switching method in two dimensions (x_1 and x_2) for three surfaces (V_1 , V_2 , and V_3) defined by simple functions. The $V_{\text{MS-ARMD}}$ surface is always the lowest-energy surface (V_{\min}), except for the region where more surfaces have similarly low energy (within a few times $\Delta V = 0.2$). Here, the algorithm switches smoothly among them as a function of the coordinates. All quantities are in arbitrary units.

3.2. Extending Flexibility of MS-ARMD PES. MS-ARMD as presented in the previous section has been implemented into the latest CHARMM version. It allows us to add/remove or reparametrize the following standard force field terms: harmonic bond, Morse bond, harmonic angle and Urey–Bradley potential, Fourier series for proper dihedral angle potentials, improper dihedral angle potential, electrostatic interactions, and the Lennard–Jones potential also with a separate parameter set for 1–4 neighbors. As the energy of each force field is measured from its own global minimum, an additive constant can be defined for each force field to level all PESs relative to each other in order to reproduce reaction energies.

The standard force field terms were devised for local small-amplitude motions of semi-rigid molecules and cannot be expected to adequately capture the dynamics far from the minimum energy structure, even with a Morse potential for the bonds. In order to increase the flexibility of the MS-ARMD force field, we introduce a generalized Lennard–Jones potential (equivalent to the Mie-potential^{30,31}) to improve the description of the van der Waals interaction between atoms in the reaction region, which also better captures the energetics for the reactant and product complexes and around the transition state.

$$V_{\text{GLJ}}(r; n, m, \varepsilon, r_{\min}) = \frac{n\varepsilon}{m-n} \left[\left(\frac{r_{\min}}{r} \right)^m - \frac{m}{n} \left(\frac{r_{\min}}{r} \right)^n \right] \quad (11)$$

The quantities ε (>0) and r_{\min} are the well depth and the separation at the energy minimum, respectively. When a bond between atoms A and B is broken, the bonded (stretch) interactions are replaced by nonbonded interactions (van der Waals and electrostatics). Because in typical force fields the sum of the van der Waals radii of two atoms is significantly larger than the equilibrium bond length between them, unphysically strong repulsions can occur upon switching. This artifact can also be avoided by using a Mie potential.

Force fields separately optimized for reactant and product states have no common zero of energy, and combining them sometimes leads to an unrealistic high-energy crossing point. In order to correctly place all PESs relative to each other in accordance with the electronic structure calculations, an additive constant Δ_i is introduced for each of the n PESs $V_i(\mathbf{x})$, which is used in fitting the global PES. As the Δ_i 's only affect the energy scale; they are not explicitly shown in the final equations. Furthermore, in order to best capture the barrier region determined from electronic structure calculations, products of Gaussian and polynomial functions (GAPO) of the energy difference $\Delta V_{ij}(\mathbf{x}) = V_j(\mathbf{x}) - V_i(\mathbf{x})$ are used. Each GAPO can be of different order $m_{ij,k}$

$$\Delta V_{\text{GAPO},k}^{ij}(\mathbf{x}) = \exp \left(- \frac{(\Delta V_{ij}(\mathbf{x}) - V_{ij,k}^0)^2}{2\sigma_{ij,k}^2} \right) \times \sum_{l=0}^{m_{ij,k}} a_{ij,kl} (\Delta V_{ij}(\mathbf{x}) - V_{ij,k}^0)^l \quad (12)$$

Here, $V_{ij,k}^0$ and $\sigma_{ij,k}$ denote the center and the standard deviation of the Gaussian function, respectively. Whenever the energy difference between the two PESs deviates from $V_{ij,k}^0$ more than a few times of $\sigma_{ij,k}$, the corresponding GAPO function will be negligible. Therefore, if $V_{ij,k}^0$ and $\sigma_{ij,k}$ are small, the correction

functions will be non-negligible only close to the crossing region and will rapidly decay away from it. In order to faithfully represent the crossing region between any two PESs i and j , a number $n_{ij} \geq 0$ of GAPOs may be required. Hence, for a system with n states described by PESs $V_i(\mathbf{x})$ ($i = 1..n$) there are $\sum_{i=1}^{n-1} \sum_{j=i+1}^n n_{ij} \geq n(n-1)/2$ GAPOs in total (eq 13). The global PES is then a weighted sum of PESs (first term in eq 13) and the sum of GAPOs weighted with the sum of the weights of the two corresponding surfaces (second term in eq 13)

$$V_{\text{MS-ARMD}}(\mathbf{x}) = \sum_{i=1}^n w_i(\mathbf{x}) V_i(\mathbf{x}) + \sum_{i=1}^{n-1} \sum_{j=i+1}^n [w_i(\mathbf{x}) + w_j(\mathbf{x})] \sum_{k=1}^{n_{ij}} \Delta V_{\text{GAPO},k}^{ij}(\mathbf{x}) \quad (13)$$

In actual MD simulations, where the gradient of the PES with respect to the coordinates is required, the term from eq 10 needs to be supplemented by the derivative of the second term in eq 13.

In summary, for the global MS-ARMD PES, the conventional FFs $V_i(\mathbf{x})$ need to be known together with optimized values for the switching (ΔV) and leveling (Δ_i) parameters and the parameters of the GAPO functions between pairs of crossing PESs ($V_{ij,k}^0$, $\sigma_{ij,k}$, $m_{ij,k}$, $a_{ij,kl}$, and n_{ij}). In the present work, these parameters are optimized with reference to electronic structure calculations. However, it would also be possible to include suitable data from experiment, as has been done before.^{32,33}

4. APPLICATION: VIBRATIONALLY INDUCED PHOTODISSOCIATION OF H_2SO_4

4.1. Force Fields for H_2SO_4 and $\text{H}_2\text{O} + \text{SO}_3$. To demonstrate the capabilities of the MS-ARMD method, we apply it to the vibrationally induced photodissociation of sulfuric acid (H_2SO_4).²⁹ Previous semi-empirical on-the-fly MD simulations have already shown that after significant vibrational excitation, H_2SO_4 can undergo two different chemical transformations including intramolecular H-transfer and water elimination ($\text{H}_2\text{SO}_4 \rightarrow \text{H}_2\text{O} + \text{SO}_3$) (Figure 5A).²⁴ In order to follow both reactions, the global PES needs to describe all

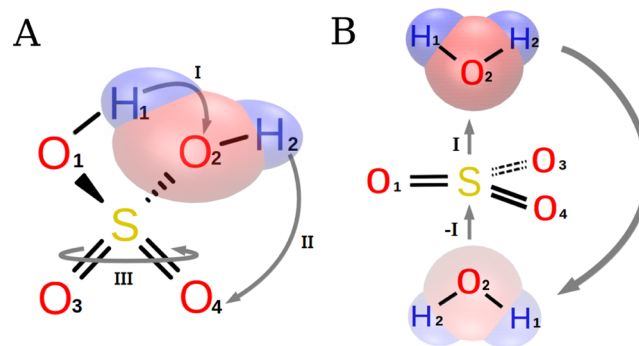


Figure 5. (A) Reactions with the three lowest barriers for sulfuric acid considered in the present work: water elimination (pathway I), H-transfer between sp^3 and sp^2 oxygen atoms (pathway II), or inversion of the bond configuration around the sulfur center (pathway III). (B) Inverted configuration of the oxygen atoms can be obtained via the low-energy pathway of elimination and subsequent addition (pathway I) of water. Readdition was not observed in our studies due to the escape of water. Oxygen and hydrogen atoms are labeled from 1 to 4 and 1 to 2 for later reference.

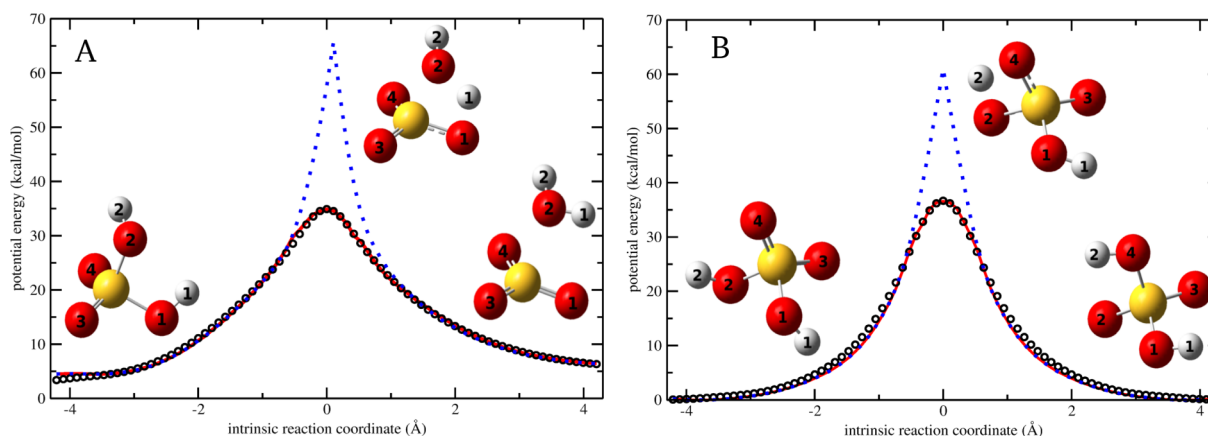


Figure 6. Potential energy along the IRC for water elimination (A) and for intramolecular H-transfer (B). Black circles are the *ab initio* reference data. The blue dotted curve corresponds to MS-ARMD surface ($\Delta V = 1$ kcal/mol) without GAPO. The red solid curve is the same with GAPOs and with the optimized $\Delta V \approx 13$ kcal/mol. Structures of stationary states along the IRCs are also shown in ball-and-stick representation.

states involved (see below). As the current work focuses on the theory and implementation of MS-ARMD, the details of fitting and thoroughly exploring the PES and the dynamics on it will be discussed elsewhere.

All electronic structure calculations were carried out at the MP2/6-311G++(2d,2p) level with the Gaussian03 suite of programs.³⁴ The energy at the equilibrium geometry of H_2SO_4 was chosen as the global zero reference for leveling all *ab initio* energies. Representative geometries for *ab initio* reference points were collected from MD simulations using previously employed FFs for H_2O , SO_3 , and H_2SO_4 .¹⁷ Starting from an optimized geometry, the system was heated to 300 K and equilibrated for 40 ps, which was followed by 10 ns of free microcanonical dynamics. Along the three trajectories, approximately 1000, 1000, and 3000 geometries were selected for H_2O , SO_3 , and H_2SO_4 , respectively. Furthermore, for H_2SO_4 , a rigid 2D scan of the H1-O1-S=O3 and H2-O2-S=O4 was performed resulting in a further 1296 ($=36^2$) reference data points that were added to the previous 3000.

The force fields for the three molecules were constructed using a Morse potential for the bonds and a harmonic potential with a Urey–Bradley potential for the angles. For SO_3 , the same improper dihedral angle potential was employed symmetrically (i.e., $\phi[\text{SO1O3O4}]$, $\phi[\text{SO3O4O1}]$, and $\phi[\text{SO4O1O3}]$), whereas for H_2SO_4 proper dihedral angle potentials were used. Coulomb interactions at the level of atomic point charges and generalized Lennard–Jones potentials (eq 11) were used between 1 and 4 and 1–5 neighboring atoms of H_2SO_4 . The initial guess for the point charges was obtained by fitting the molecular electrostatic potential on a grid using the CHELPG scheme.³⁵ Initial values for all other parameters were taken or calculated (i.e., for generalized Lennard–Jones) from standard CHARMM parameters. A standalone Fortran code based on the downhill simplex algorithm³⁶ was used for optimizing all force field and surface-leveling parameters to match the *ab initio* reference energies. The final RMSDs were 0.02, 0.47, and 1.23 kcal/mol for H_2O , SO_3 , and H_2SO_4 , respectively.

For the $\text{H}_2\text{O} \cdots \text{SO}_3$ van der Waals complex, separate MD simulations were carried out at 300 K, and 2000 geometries were sampled for electronic structure calculations. The nonbonded terms, including parameters for generalized Lennard–Jones potentials and point charges, were optimized, while the bonded parameters, refined above, remained

unchanged. The final RMSD of this fit was 0.55 kcal/mol. Such accuracy in fitting several thousand reference points has also been found in previous work.²⁵

4.2. Parametrization of Minimum Energy Paths. For quantitative simulations of the reactions of interest, the global PES also has to describe the barrier regions adequately. One possibility is to determine the minimum energy paths (MEPs) from the transition state leading to either reactant or product. This was done by first locating the transition states from quadratic synchronous transit (QST) calculations,³⁷ followed by an intrinsic reaction coordinate (IRC) calculation. The two minimum energy paths for water elimination and intramolecular H-transfer are shown in Figure 6. The reference *ab initio* calculations yield a barrier height of 32.0 kcal/mol for water elimination, and 36.6 kcal/mol for intramolecular H-transfer, which also supports that the latter process is competitive and should be included for realistic simulations. In previous computational studies, the energy barrier for water elimination has been found to be in the range of 32–40 kcal/mol depending on the level of theory used.^{17,27,38} The system can be involved in another nondissociative chemical transformation, namely, the inversion of the bond configuration around the sulfur center (Figure 5 B). A corresponding transition state calculation finds a barrier height of 90.4 kcal/mol that makes this process highly improbable compared to the other two transformations. Hence, it is not considered any further.

Figure 6 compares the energy along the IRCs from the electronic structure calculations with those from the MS-ARMD force field. Evidently, the global separately parametrized FFs for H_2SO_4 and $\text{H}_2\text{O} \cdots \text{SO}_3$ lead to barrier heights 20–30 kcal/mol higher than the reference data (dotted line). To better capture the barrier region, GAPO functions were used. For this, the parameters in the GAPO functions, the switching parameter ΔV , and the overall shift of the FFs were optimized. Using three GAPOs with first-order polynomials for the H_2O elimination and two GAPOs with second-order polynomials for the H-transfer reactions, the energy profile along the reference MEP can be reproduced very closely (RMSD = 0.55 kcal/mol), as is shown in Figure 6 (red continuous line).

4.3. Construction of Permutation Invariant Surface. In force fields, atom indices are used to define the connectivity of atoms. Intramolecular H-transfer in sulfuric acid of a given atom indexing can give four additional states that differ only in

the oxygen–atom indices to which the transferred H-atom is bound. Water elimination from sulfuric acid of a given atom indexing can lead to $\text{H}_2\text{O} + \text{SO}_3$ states with two different indexing of atoms. All possible H_2SO_4 states and the $\text{H}_2\text{O} + \text{SO}_3$ states are separately chemically equivalent to each other; therefore, they have to have exactly the same FF parametrization. The only difference being that the indices of some oxygen atoms involved in the H-transfer are swapped, and the signs of the $\text{H}-\text{O}-\text{S}=\text{O}$ dihedral angles potential phases need to be chosen accordingly. The global PES has to describe all these equivalent states with all possible reaction pathways between them. For this, copies of surfaces and sets of GAPO functions are used.

Altogether, 16 states (4^2) can then be distinguished by a two-digit index (e.g., 12, or 34) that denotes to which O-atoms the two H-atoms, H1 and H2, are bound (for atom labels, see Figure 5). Two identical digits (e.g., 11, or 22) represent a state in which the H-atoms are bound to the same O-atom, i.e., an H_2O molecule corresponding to the dissociated state $\text{H}_2\text{O} + \text{SO}_3$. In the present gas-phase, single-molecule, free-dynamics studies, the water molecule escapes after elimination from H_2SO_4 , and there is no possibility for recombination with the SO_3 molecule. In situations where the reaction products reform H_2SO_4 , the global PES would need to support the possibility for addition of H_2O also to the other side of the SO_3 molecule (“top” and “bottom” side; Figure 5B). The resulting sulfuric acid molecule is a mirror image of the other with respect to the configuration of the oxygen atoms. It would require 12 more copies of the sulfuric acid PESs that are identical except for the phases of the $\text{H}-\text{O}-\text{S}=\text{O}$ dihedral angle potentials, which all would reverse their sign. To describe these mirror image configurations without adding further surfaces, we chose the phase shifts of all dihedral angle potentials within sulfuric acid to be either 0° or 180° ($\equiv -180^\circ$). Therefore our final surface can describe the states and reactions of all possible configurations of sulfuric acid.

The network of states (vertices) and possible reactions (edges) between them can be represented as a graph (Figure 7). Each state can be involved in six (degree of the vertex) different reactions during which one of their digits changes to one of the three other possibilities (e.g., $11 \rightarrow 21, 31, 41, 12, 13, 14$). Therefore, each state can be reached from any other state in two reaction steps (diameter of a graph). Hence, the reaction network corresponds to a symmetric graph with 16 equivalent vertices of degree 6, with a diameter of 2, as shown in Figure 7. The 16-state reaction network has altogether 48 edges corresponding to 48 transition states, of which 24 involve H-transfer and 24 correspond to H_2O -elimination. In summary, the global surface, which is invariant to the permutation of chemically equivalent atoms, was generated from 12 H_2SO_4 surfaces and 4 $\text{H}_2\text{O}+\text{SO}_3$ surfaces and 48 ($24 + 24$) sets of GAPO functions.

4.4. Vibrational Excitation and Reaction Dynamics.

The dynamics of sulfuric acid after OH vibrational overtone excitation was investigated in order to validate the MS-ARMD implementation in CHARMM. Starting from the optimized H_2SO_4 geometry, the molecule was heated to 300 K in 20 ps, equilibrated for 30 ps, and evolved freely for 20 ps, which was followed by vibrational excitation (see below). The equations of motion were propagated using the leapfrog Verlet algorithm with a time step of $\Delta t = 0.1$ fs. Vibrational excitation was invoked by scaling the instantaneous velocities along the ν_9 normal mode, which corresponds approximately to the OH-

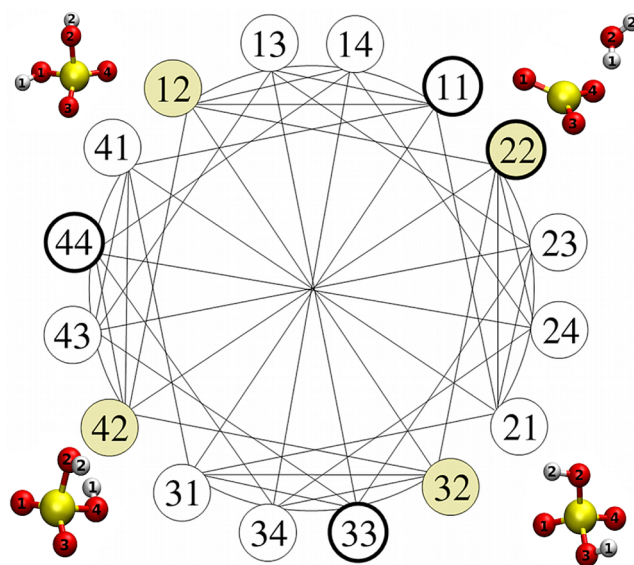


Figure 7. Network of states (vertices, circles) and possible reactions (lines) for H_2SO_4 represented as a symmetric graph. States are denoted by circles and labeled by a two-digit index, see text. Allowed reactions at the investigated energies are intramolecular H-transfer and H_2O -elimination. The four states observed in a typical trajectory (Figure 8) are highlighted and given as a ball-and-stick representation. Four thick-line circles correspond to states of $\text{H}_2\text{O} + \text{SO}_3$.

stretching local mode even in highly excited states. For the present simulations, 5 quanta of vibrational energy, corresponding to 47.15 kcal/mol, were deposited into this mode,^{17,39} which is significantly larger than the average total thermal energy of H_2SO_4 of ≈ 9 kcal/mol at 300 K. After excitation, propagation continued for 500 ps or until water elimination took place. Overall, 50 independent trajectories were run.

Figure 8 reports the total energy along a part of one typical such trajectory. Three intramolecular H-transfer processes were observed at times 15, 30, and 63 ps, which were eventually followed by water elimination at 132 ps. Figure 8 also shows the transition times and the states visited.

The energy fluctuations of up to ± 0.06 kcal/mol at the beginning of the excited trajectory are due to the localization of the large excess energy in a single OH-stretching mode. The rapid motion of the H atoms cannot be described accurately with the stepsize, especially at the short bond length turning point. This could be improved by using an adaptive integrator, which was done in our previous work.²⁵ But even with a Verlet-type integrator, as is commonly used in biomolecular simulations, the degree of energy conservation is sufficient for large-scale applications. Once the excitation energy has been redistributed, particularly into the hindered $\text{O}=\text{S}-\text{O}-\text{H}$ rotations, the fluctuations decrease, which occurs after 15 ps for the particular trajectory shown in Figure 8. After the hindered rotations gain sufficient energy to surpass their barriers, the optimal conformations for H-transfer and water elimination can be accessed. Before each crossing, an increase in the energy fluctuations can be observed, which originates from a relocation of energy into one of the OH-stretching modes. Throughout the course of several H-transfer reactions and the final water elimination step, no drift in the total energy occurs, which validates the present implementation in CHARMM.

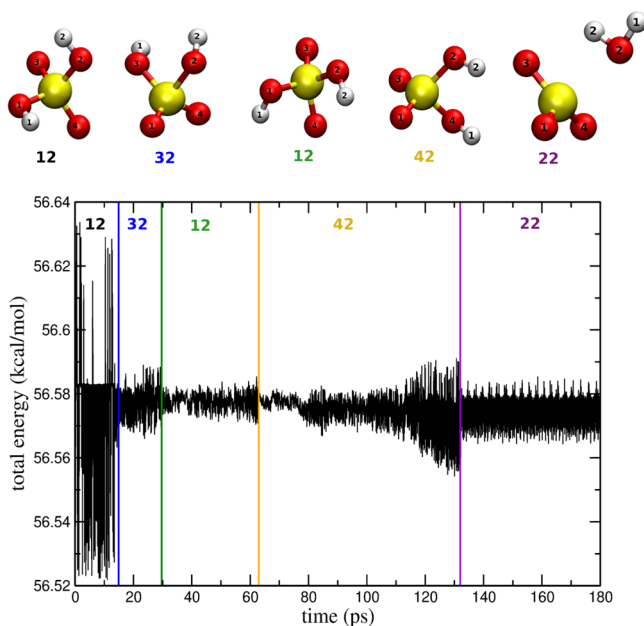


Figure 8. Total energy as a function of time for a simulation with several reactive steps. The significant fluctuations during the first 15 ps are caused by the initial preparation of the $\nu_9 = 5$ state, which contains a significant amount of energy in a single OH-stretching mode. The two-digit labels refer to the state of the system (Figure 7), and the ball-and-stick models are corresponding representative structures.

For further statistical characterization, a histogram of the root-mean-square energy fluctuation ($E_i - \langle E \rangle$, $i = 1$ to 50) for all 50 trajectories was constructed and analyzed. This probability distribution ($\rho(E - \langle E \rangle)$) is shown in Figure 9. The distribution ρ has an expectation value of $\mu = 0$, and the standard deviation is $\sigma = 0.0073$ kcal/mol. The corresponding Gaussian distribution $\rho(x) = \exp[-(x - \mu)^2/2\sigma^2]/(2\pi)^{1/2}\sigma$ is also shown in Figure 9. In summary, we conclude that stable energy-conserving simulations can be carried out with MS-

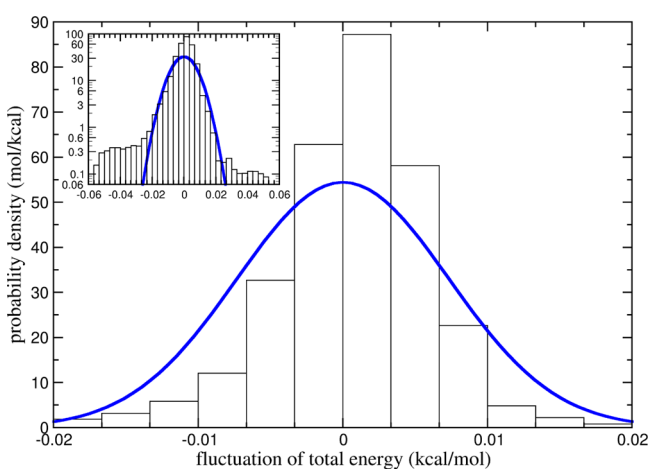


Figure 9. Distribution of total energy fluctuations based on simulations of the free dynamics of sulfuric acid after excitation of the OH-stretching overtone ($\nu_9 = 5$) for 50 independent initial conditions sampled at 300 K. Standard deviation $\sigma = 0.0073$ kcal/mol was empirically estimated from the sample, and the corresponding Gaussian distribution is also plotted. Note the expectation value (μ) of the fluctuation is 0 by definition.

ARMD on the nanosecond time scale even for such a highly excited system.

5. DISCUSSION AND CONCLUSIONS

In the present manuscript, we have presented a multisurface energy conserving generalization of the ARMD algorithm. It allows us to construct global reactive PESs by smoothly connecting parametrized FFs involving several states. The MS-ARMD method was implemented in version c39a2 of CHARMM in a general way.

The computational investigation of chemical reaction dynamics is also possible by using *ab initio* molecular dynamics (AIMD) methods. Such approaches have been successfully applied to characterizing rapid reactions (e.g., photochemical processes or proton transfer)^{40–43} or individual reaction pathways for complex systems such as proteins.^{44–47} Evidently, the computational time required for such simulations directly depends on the level of the electronic structure method employed, which in turn determines the accuracy with which such processes can be followed. Hence, for small systems (such as H_2SO_4 or H_5O_2^+ in the gas phase),^{24,48} individual trajectories at the correlated level (MP2) with explicit atom-centered basis sets can be envisaged. For larger systems, such as protein active sites, a mixed quantum mechanical (QM)/molecular mechanics (MM) ansatz needs to be employed together with density functional theory or semi-empirical methods.^{49–51}

If, however, converged reaction rates—instead of single illustrative reactive trajectories—are of interest, the computational burden of AIMD simulations is too large, as running long-time and multiple (several hundred to several thousand) independent trajectories is impractical even with today's computational architectures and their development in the nearer future. As an example, based on the CPU timing (eight processors) of an exploratory 100 step AIMD simulation of H_2SO_4 using MP2/6-311G++(2d,2p)—the level at which the *ab initio* reference points were determined in the present work—with a time step of $\Delta t = 0.25$ fs, the expected CPU time for a 1 ns trajectory is approximately 3 months. Also, if reaction rates are to be determined from Monte Carlo-based methods (such as path integral MC), several million energy evaluations are required for converged results, which prevents the routine use of *ab initio* or DFT-based methods even for relatively small systems such as malonaldehyde.^{6,52} For these applications, force field-based methods are ideally suited. The time-limiting factor in this case is the fitting of suitably parametrized PESs, which allows rapid energy and force evaluations. However, as shown in the present work, this is possible, although additional and convenient computational tools for routine fitting of parametrized PESs will need to be further developed.^{33,53} Alternatively, with the advent of powerful numerical methods, representations of multidimensional PESs have become possible, at least for low-dimensional systems.^{54–57} A final and important benefit of parametrized FFs (not only in applications to chemical reactions) is the fact that they do not need to rely solely on electronic structure reference data but that fitting them may also include experimental observables (such as structures or vibrational frequencies) complementary to the properties of interest.³³

Other reactive molecular dynamics methods based on empirical force fields have been recently and thoroughly reviewed.^{18,58} A general and widely used procedure is the Empirical Valence Bond Model (EVB),¹³ which requires the lowest eigenvalue of an $n \times n$ matrix if n states are involved to

obtain the effective PES. This usually needs to be done numerically, which can become computationally prohibitive. On the contrary, for MS-ARMD, the time for evaluating energies and forces scales linearly with the number of low-lying surfaces. By construction, the MS-ARMD surface always passes through or above the crossing point, whereas the EVB surface always is below the crossing point. Furthermore, with the help of Gaussian and polynomial product functions, the MS-ARMD PES is very flexible to reproduce reference data in the barrier region. As a future development, it will also be possible to replace the GAPO functions by single-variable tabulated functions. The MS-ARMD algorithm can also be extended with Gaussian or Gaussian times a polynomial functions of the coordinates, similar to the Chang-Miller⁵⁹ and the distributed Gaussian⁶⁰ extension of EVB, to adjust the frequencies of stationary states or the shape of PES around any selected geometry locally.

To validate the implementation, H-transfer and water elimination in H₂SO₄ induced by high vibrational excitation of the OH-stretching mode was investigated. The MS-ARMD algorithm was used for constructing a permutationally invariant PES for sulfuric acid based on 12 H₂SO₄ and 4 H₂O + SO₃ force fields. The trajectories establish that total energy is conserved on the nanosecond time scale during which several reactive processes take place. The present implementation in CHARMM allows modeling of chemical reactions including gas-phase reactions of small molecules, homogeneous and heterogeneous catalytic reactions, and enzyme catalysis. Hence, the functionality is comparable to that of QM/MD albeit at approximately the speed of a conventional force field simulation. The additional required effort is evidently the parametrization of the force fields involved.

AUTHOR INFORMATION

Corresponding Authors

*E-mail: tibornagy@chem.elte.hu (T.N.).

*E-mail: m.meuwly@unibas.ch (M.M.).

Notes

The authors declare no competing financial interest.

ACKNOWLEDGMENTS

This work was supported by the Swiss National Science Foundation through Grant 200021-117810, NCCR MUST (to M.M.), and EU-COFUND program (to T.N.). The authors are grateful to Dr. Stephan Lutz, Dr. Myung Won Lee, and Dr. Tristan Bereau for insightful discussions.

REFERENCES

- (1) Hwang, J.; Warshel, A. How important are quantum mechanical nuclear motions in enzyme catalysis? *J. Am. Chem. Soc.* **1996**, *118*, 11745–11751.
- (2) Hinsen, K.; Roux, B. Potential of mean force and reaction rates for proton transfer in acetylacetone. *J. Chem. Phys.* **1997**, *106*, 3567–3577.
- (3) Pavese, M.; Chawla, S.; Lu, D.; Lobaugh, J.; Voth, G. A. Quantum effects and the excess proton in water. *J. Chem. Phys.* **1997**, *107*, 7428–7432.
- (4) Miller, W. H.; Zhao, Y.; Ceotto, M.; Yang, S. Quantum instanton approximation for thermal rate constants of chemical reactions. *J. Chem. Phys.* **2003**, *119*, 1329–1342.
- (5) Wong, K. F.; Sonnenberg, J. L.; Paesani, F.; Yamamoto, T.; Vanicek, J.; Zhang, W.; Schlegel, H. B.; Case, D. A.; Cheatham, T. E., III; Miller, W. H.; Voth, G. A. Proton transfer studied using a combined ab initio reactive potential energy surface with quantum path integral methodology. *J. Chem. Theory Comput.* **2010**, *6*, 2566–2580.
- (6) Huang, J.; Buchowiecki, M.; Nagy, T.; Vanicek, J.; Meuwly, M. Kinetic isotope effect in malonaldehyde determined from path integral Monte Carlo simulations. *Phys. Chem. Chem. Phys.* **2014**, *16*, 204–211.
- (7) Car, R.; Parrinello, M. Unified approach for molecular-dynamics and density-functional theory. *Phys. Rev. Lett.* **1985**, *55*, 2471–2474.
- (8) Herbert, J.; Head-Gordon, M. Accelerated, energy-conserving Born–Oppenheimer molecular dynamics via Fock matrix extrapolation. *Phys. Chem. Chem. Phys.* **2005**, *7*, 3269–3275.
- (9) Niklasson, A. M.; Tymczak, C. J.; Challacombe, M. Time-reversible Born–Oppenheimer molecular dynamics. *Phys. Rev. Lett.* **2006**, *97*, 123001.
- (10) Warshel, A.; Levitt, M. Theoretical studies of enzymic reactions: Dielectric, electrostatic and steric stabilization of the carbonium ion in the reaction of lysozyme. *J. Mol. Biol.* **1976**, *103*, 227–249.
- (11) Field, M. J.; Bash, P. A.; Karplus, M. A combined quantum-mechanical and molecular mechanical potential for molecular-dynamics simulations. *J. Comput. Chem.* **1990**, *11*, 700–733.
- (12) Bash, P. A.; Field, M. J.; Karplus, M. Free energy perturbation method for chemical reactions in the condensed phase: A dynamic approach based on a combined quantum and molecular mechanics potential. *J. Am. Chem. Soc.* **1987**, *109*, 8092–8094.
- (13) Warshel, A.; Weiss, R. M. An empirical valence bond approach for comparing reactions in solutions and in enzymes. *J. Am. Chem. Soc.* **1980**, *102*, 6218–6226.
- (14) Danielsson, J.; Meuwly, M. Atomistic simulation of adiabatic reactive processes based on multi-state potential energy surfaces. *J. Chem. Theory Comput.* **2008**, *4*, 1083–1093.
- (15) Mishra, S.; Meuwly, M. Atomistic simulation of NO dioxygenation in group I truncated hemoglobin. *J. Am. Chem. Soc.* **2010**, *132*, 2968–2982.
- (16) Rivera, C. A.; Winter, N.; Harper, R. V.; Benjamin, I.; Bradforth, S. E. The dynamical role of solvent on the ICN photodissociation reaction: connecting experimental observables directly with molecular dynamics simulations. *Phys. Chem. Chem. Phys.* **2011**, *13*, 8269–8283.
- (17) Yosa, J.; Meuwly, M. Vibrationally induced dissociation of sulfuric acid (H₂SO₄). *J. Phys. Chem. A* **2011**, *115*, 14350–14360.
- (18) Farah, K.; Mueller-Plathe, F.; Boehm, M. C. Classical reactive molecular dynamics implementations: State of the art. *Chem. Phys. Chem.* **2012**, *13*, 1127–1151.
- (19) Schmitt, U.; Voth, G. Multistate empirical valence bond model for proton transport in water. *J. Phys. Chem. B* **1998**, *102*, 5547–5551.
- (20) Hong, G.; Rosta, E.; Warshel, A. Using the constrained DFT approach in generating diabatic surfaces and off diagonal empirical valence bond terms for modeling reactions in condensed phases. *J. Phys. Chem. B* **2006**, *110*, 19570–19574.
- (21) Nutt, D. R.; Meuwly, M. Studying reactive processes with classical dynamics: Rebinding dynamics in MbNO. *Biophys. J.* **2006**, *90*, 1191–1201.
- (22) Dayal, P.; Weyand, S. A.; McNeish, J.; Mosey, N. J. Temporal quantum mechanics/molecular mechanics: Extending the time scales accessible in molecular dynamics simulations of reactions. *Chem. Phys. Lett.* **2011**, *516*, 263–267.
- (23) Nienhaus, K.; Lutz, S.; Meuwly, M.; Nienhaus, G. U. Reaction-pathway selection in the structural dynamics of a heme protein. *Chem.—Eur. J.* **2013**, *19*, 3558–3562.
- (24) Miller, Y.; Gerber, R. B. Dynamics of vibrational overtone excitations of H₂SO₄, H₂SO₄·H₂O: Hydrogen-hopping and photodissociation processes. *J. Am. Chem. Soc.* **2006**, *128*, 9594–9595.
- (25) Tong, X.; Nagy, T.; Yosa, J.; Germann, M.; Meuwly, M.; Willitsch, S. State-selected ion–molecule reactions with Coulomb-crystallized molecular ions in traps. *Chem. Phys. Lett.* **2012**, *547*, 1–8.
- (26) Clement, C. F.; Ford, I. J. Gas-to-particle conversion in the atmosphere: I. Evidence from empirical atmospheric aerosols. *Atmos. Environ., Part A* **1999**, *33*, 475–487.
- (27) Larson, L. J.; Kuno, M.; Tao, F. M. Hydrolysis of sulfur trioxide to form sulfuric acid in small water clusters. *J. Chem. Phys.* **2000**, *112*, 8830–8838.

- (28) Donaldson, D.; Frost, G.; Rosenlof, K.; Tuck, A. F.; Vaida, V. Atmospheric radical production by excitation of vibrational overtones via absorption of visible light. *Geophys. Res. Lett.* **1997**, *24*, 2651–2654.
- (29) Vaida, V.; Kjaergaard, H. G.; Hintze, P. E.; Donaldson, D. J. Photolysis of sulfuric acid vapor by visible solar radiation. *Science* **2003**, *299*, 1566–1568.
- (30) Mie, G. Zur kinetischen Theorie der einatomigen Körper. *Ann. Phys.* **1903**, *11*, 657–697.
- (31) Kramer, C.; Gedeck, P.; Meuwly, M. Multipole-based force fields from ab initio interaction energies and the need for jointly refitting all intermolecular parameters. *J. Chem. Theory Comput.* **2013**, *9*, 1499–1511.
- (32) Meuwly, M.; Hutson, J. M. *J. Chem. Phys.* **1999**, *110*, 8338.
- (33) Devereux, M.; Meuwly, M. Force field optimization using dynamics and ensemble-averaged data: Vibrational spectra and relaxation in bound MbCO. *J. Chem. Inf. Model.* **2010**, *50*, 349–357.
- (34) Frisch, M. J.; Trucks, G. W.; Schlegel, H. B.; Scuseria, G. E.; Robb, M. A.; Cheeseman, J. R.; Montgomery, J. A. J.; Vreven, T.; Kudin, K. N.; Burant, J. C.; Millam, J. M.; Iyengar, S. S.; Tomasi, J.; Barone, V.; Mennucci, B.; Cossi, M.; Scalmani, G.; Rega, N.; Petersson, G. A.; Nakatsuji, H.; Hada, M.; Ehara, M.; Toyota, K.; Fukuda, R.; Hasegawa, J.; Ishida, M.; Nakajima, T.; Honda, Y.; Kitao, O.; Nakai, H.; Klene, M.; Li, X.; Knox, J. E.; Hratchian, H. P.; Cross, J. B.; Adamo, C.; Jaramillo, J.; Gomperts, R.; Stratmann, R. E.; Yazyev, O.; Austin, A. J.; Cammi, R.; Pomelli, C.; Ochterski, J. W.; Ayala, P. Y.; Morokuma, K.; Voth, G. A.; Salvador, P.; Dannenberg, J. J.; Zakrzewski, V. G.; Dapprich, S.; Daniels, A. D.; Strain, M. C.; Farkas, O.; Malick, D. K.; Rabuck, A. D.; Raghavachari, K.; Foresman, J. B.; Ortiz, J. V.; Cui, Q.; Baboul, A. G.; Clifford, S.; Cioslowski, J.; Stefanov, B. B.; Liu, G.; Liashenko, A.; Piskorz, P.; Komaromi, I.; Martin, R. L.; Fox, D. J.; Keith, T.; Al-Laham, M. A.; Peng, C. Y.; Nanayakkara, A.; Gonzalez, C.; Challacombe, M.; Gill, P. M. W.; Johnson, B.; Chen, W.; Wong, M. W.; Andres, J. L.; Gonzalez, C.; Head-Gordon, M.; Replogle, E. S.; Pople, J. A. Gaussian 03, Revision C.01. Gaussian, Inc., Wallingford CT, 2004.
- (35) Breneman, C. M.; Wiberg, K. B. Determining atom-centered monopoles from molecular electrostatic potentials. The need for high sampling density in formamide conformational analysis. *J. Comput. Chem.* **1990**, *11*, 361–373.
- (36) Nelder, J.; Mead, R. A simplex method for function minimization. *Chem. Phys.* **1965**, *7*, 308–313.
- (37) Halgren, T.; Lipscomb, W. The synchronous-transit method for determining reaction pathways and locating molecular transition states. *Chem. Phys. Lett.* **1977**, *49*, 225–232.
- (38) Morokuma, K.; Muguruma, C. Ab initio molecular orbital study of the mechanism of the gas phase reaction $\text{SO}_3 + \text{H}_2\text{O}$: Importance of the second water molecule. *J. Am. Chem. Soc.* **1994**, *116*, 10316–10317.
- (39) Nguyen, P. N.; Stock, G. Nonequilibrium molecular-dynamics study of the vibrational energy relaxation of peptides in water. *J. Chem. Phys.* **2003**, *119*, 11350–11358.
- (40) Tavernelli, I.; Curchod, B.; Rothlisberger, U. Nonadiabatic molecular dynamics with solvent effects: A LR-TDDFT QM/MM study of ruthenium (II) tris (bipyridine) in water. *Chem. Phys.* **2011**, *391*, 101–109.
- (41) Sagnella, D. E.; Laasonen, K.; Klein, M. L. Ab initio molecular dynamics study of proton transfer in a polyglycine analog of the ion channel gramicidin A. *Biophys. J.* **1996**, *71*, 1172–1178.
- (42) Tuckerman, M. E.; Marx, D.; Klein, M.; Parrinello, M. On the quantum nature of the shared proton in hydrogen bonds. *Science* **1997**, *275*, 817–820.
- (43) Marx, D.; Tuckerman, M. E.; Jurg, H.; Parrinello, M. The nature of the hydrated excess proton in water. *Nature* **1999**, *397*, 601–604.
- (44) Wong, K.; Gao, J. The reaction mechanism of paraoxon hydrolysis by phosphotriesterase from combined QM/MM simulations. *Biochemistry* **2007**, *46*, 13352–13369.
- (45) Lonsdale, R.; Houghton, K. T.; Åzurek, J.; Bathelt, C. M.; Foloppe, N.; de Groot, M. J.; Harvey, J. N.; Mulholland, A. J. Quantum mechanics/molecular mechanics modeling of regioselectivity of drug metabolism in cytochrome P450 2C9. *J. Am. Chem. Soc.* **2013**, *135*, 8001–8015.
- (46) Zhan, C.; Gao, D. Catalytic mechanism and energy barriers for butyrylcholinesterase-catalyzed hydrolysis of cocaine. *Biophys. J.* **2005**, *89*, 3863–3872.
- (47) Senn, H. M.; Thiel, W. QM/MM methods for biomolecular systems. *Angew. Chem. Intern. Ed.* **2009**, *48*, 1198–1229.
- (48) Vener, M. V.; Sauer, J. Environmental effects on vibrational proton dynamics in H_2O_2^+ : DFT study on crystalline $\text{H}_2\text{O}_2+\text{ClO}_4^-$. *Phys. Chem. Chem. Phys.* **2005**, *7*, 258–263.
- (49) Field, M. J.; Bash, P. A.; Karplus, M. A combined quantum mechanical and molecular mechanical potential for molecular dynamics simulations. *J. Comput. Chem.* **1990**, *11*, 700–733.
- (50) Dapprich, S.; Komaromi, I.; Byun, K.; Morokuma, K.; Frisch, M. A new ONIOM implementation in Gaussian98. Part I. The calculation of energies, gradients, vibrational frequencies and electric field derivatives. *J. Mol. Struct.: THEOCHEM* **1999**, *461*–462, 1–21.
- (51) Cui, Q.; Elstner, M.; Kaxiras, E.; Frauenheim, T.; Karplus, M. A QM/MM implementation of the self-consistent charge density functional tight binding (SCC-DFTB) method. *J. Phys. Chem. B* **2001**, *105*, 569–585.
- (52) Wong, K. F.; Sonnenberg, J. L.; Paesani, F.; Yamamoto, T.; Vanicek, J.; Zhang, W.; Schlegel, H. B.; Case, D. A.; Cheatham, T. E.; Miller, W. H.; Voth, G. A. Proton transfer studied using a combined ab initio reactive potential energy surface with quantum path integral methodology. *J. Chem. Theory Comput.* **2010**, *6*, 2566–2580.
- (53) Kramer, C.; Bereau, T.; Spinn, A.; Liedl, K. R.; Gedeck, P.; Meuwly, M. Deriving static atomic multipoles from the electrostatic potential. *J. Chem. Inf. Model.* **2013**, *53*, 3410–3417.
- (54) Ho, T.; Rabitz, H. A general method for constructing multidimensional molecular potential energy surfaces from abinitio calculations. *J. Chem. Phys.* **1996**, *104*, 2584–2597.
- (55) Ho, T.; Hollebeek, T.; Rabitz, H.; Harding, L. B.; Schatz, G. C. A global H_2O potential energy surface for the reaction $\text{O}(\text{1D})+\text{H}_2\text{O} \rightarrow \text{H} + \text{H}_2\text{O}$. *J. Chem. Phys.* **1996**, *105*, 10472–10486.
- (56) Meuwly, M.; Hutson, J. M. The potential energy surface and near-dissociation states of He-H_2^+ . *J. Chem. Phys.* **1999**, *110*, 3418–3427.
- (57) Braams, B. J.; Bowman, J. M. Permutationally invariant potential energy surfaces in high dimensionality. *Int. Rev. Phys. Chem.* **2009**, *28*, 577–606.
- (58) Cazade, P. A.; Huang, J.; Yosa, J.; Szymczak, J.; Meuwly, M. Atomistic simulations of reactive processes in the gas- and condensed-phase. *Int. Rev. Phys. Chem.* **2012**, *31*, 235–264.
- (59) Chang, Y.-T.; Miller, W. H. An empirical valence bond model for constructing global potential energy surfaces for chemical reactions of polyatomic molecular systems. *J. Phys. Chem.* **1990**, *94*, 5884–5888.
- (60) Schlegel, H. B.; Sonnenberg, J. L. Empirical valence-bond models for reactive potential energy surfaces using distributed gaussians. *J. Chem. Theory Comput.* **2006**, *2*, 905–911.